

# PHYSICAL DESIGN FOR SURFACE-MICROMACHINED MEMS

Gary K. Fedder<sup>†\*</sup> and Tamal Mukherjee<sup>†</sup>

<sup>†</sup>Department of Electrical and Computer Engineering and <sup>\*</sup>The Robotics Institute  
Carnegie Mellon University  
Pittsburgh, PA, 15213-3890

E-mail: fedder@ece.cmu.edu, tamal@ece.cmu.edu

## ABSTRACT

We are developing physical design tools for surface-micromachined MEMS, such as polysilicon microstructures built using MCNC's Multi-User MEMS Process service. Our initial efforts include automation of layout synthesis and behavioral simulation from a MEMS schematic representation. As an example, layout synthesis of a folded-flexure electrostatic comb-drive microresonator is demonstrated. Lumped-parameter electromechanical models with two mechanical degrees-of-freedom link the physical and behavioral parameters of the microresonator. Simulated annealing is used to generate global optimized layouts of five different resonators from 3 kHz to 300 kHz starting with mixed-domain behavioral specifications and constraints. Development of the synthesis tool enforces codification of all relevant MEMS design variables and constraints. The synthesis approach allows a rapid exploration of MEMS design issues.

## 1. INTRODUCTION

Microelectromechanical systems (MEMS) are commonly defined as sensor and actuator systems that are made using integrated-circuit fabrication processes. The main advantage of MEMS-based systems when compared with conventional electromechanical systems is the miniaturization and integration of multiple sensors, actuators, and electronics at a low cost. These attributes are obtained by leveraging standard integrated-circuit batch-fabrication processes.

In the past, MEMS technology has primarily been driven by the development of new processes to meet specific needs. However, over the past decade there has been a shift in emphasis from process design to device design. There is a growing demand for CAD tools to support rapid design of complex MEMS involving physical interactions between mechanical, electrostatic, magnetic, thermal, fluidic, and optical

domains. Several groups are addressing the deficiency in MEMS design tools, including MEMCAD [1] (Microcosm/M.I.T.), IntelliCAD [2] (IntelliSense Corp.), and CAEMEMS [3] (Univ. of Michigan). These tools focus on analysis using 3D modeling from layout and process integrated with self-consistent electromechanical numerical simulation.

In a complementary approach to existing analysis tools, we are developing circuit-level design tools and layout synthesis tools tailored to general surface-micromachined systems. The planar '2 1/2-D' topology of surface-micromachined MEMS lends itself to abstraction at a higher level than numerical simulation. As in circuit design, a schematic representation of MEMS provides a critical link between layout and behavioral simulation that enables high-level design automation. Many existing surface-micromechanical designs can be partitioned into discrete components, such as beam springs, plate masses, and electrostatic actuators, that are modeled as lumped-parameter elements. Conversely, new MEMS devices can be created by connecting together these lumped elements.

In this paper, we will describe initial work involving the rapid layout synthesis of a surface-micromachined resonator from high-level design specifications and constraints. Our approach to layout synthesis involves modeling the design problem as a formal numerical synthesis problem, and then solving it with powerful optimization techniques. This synthesis philosophy has been successful in a variety of fields such as analog circuit synthesis [4] and chemical plant synthesis [5]. The process of modeling the design problem involves determining the design variables, the numerical design constraints and the quantitative design objective. The microresonator architecture used in this study has been thoroughly analyzed in the literature. It represents a good starting point for synthesis work since proper operation can be easily veri-

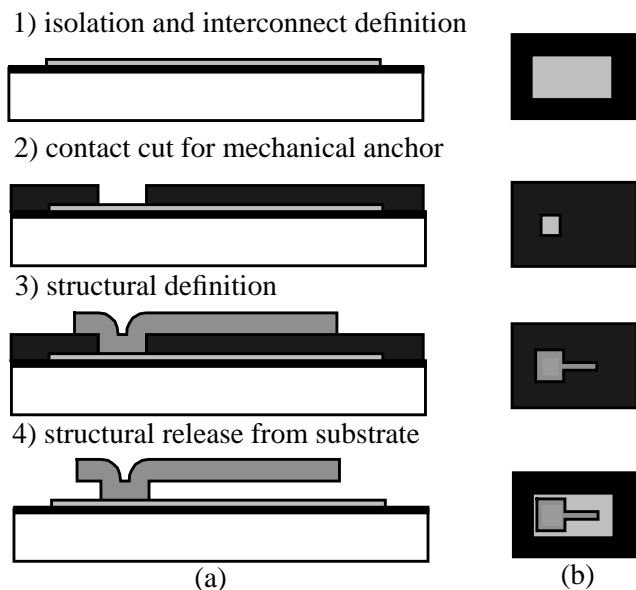


Fig. 1. Abbreviated process flow for MCNC's Multi-User MEMS Process service. (a) Cross-sectional view. (b) Top view (layout).

fied using existing analysis tools and experimental measurements.

We begin with an overview of surface-micromachining and the microresonator architecture, followed by a description of design variables and lumped-parameter models. Next, the design constraints are specified along with the synthesis algorithm and a discussion of the layout synthesis results.

## 2. MICRORESONATOR DESCRIPTION

### 2.1. Surface Micromachining

One set of events that has fueled the trend toward device design in fixed processes is the establishment of MEMS process services by MCNC [6], Analog Devices [7], CMP [8], and MOSIS [9] (Currently, post-foundry processing is required for MOSIS designs). These services produce micromechanical structures made out of thin films on the surface of the substrate. We refer to these thin-film microstructures as 'surface-micromachined MEMS' although, in some cases, bulk silicon micromachining is required to release the microstructures from the substrate.

MCNC's Multi-user MEMS Process service (MUMPs) is the technology chosen for the synthesis work presented in this paper. A simplified and truncated process flow is shown in Fig. 1. Low-stress sili-

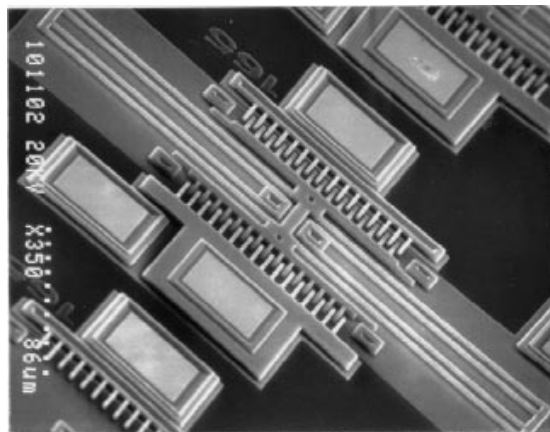


Fig. 2. Scanning electron micrograph of a released folded-flexure comb-drive microresonator fabricated in the MUMPs process.

con nitride is first deposited on the silicon substrate to provide electrical isolation between microstructures. An electrical interconnect layer of polycrystalline silicon (polysilicon) is then deposited and patterned. Next, a  $2\text{ }\mu\text{m}$ -thick layer of phosphosilicate glass (PSG) is deposited. The PSG acts as a sacrificial spacer layer for the microstructures. After contact cuts are made in the PSG, a  $2\text{ }\mu\text{m}$ -thick layer of polysilicon is deposited and patterned to form the microstructures. Further process steps in MUMPs are not necessary for microresonator fabrication and will not be shown. A final wet etch in hydrofluoric acid (HF) dissolves the PSG and releases the microstructure so it is free to move. The PSG contact cuts act as mechanical anchor points that fix the microstructure to the substrate surface.

### 2.2. Microresonator Design

A microresonator fabricated in MUMPs is shown in Fig. 2. The specific microresonator design was first described and analyzed by Tang [10] and is commonly used as for MEMS process characterization. In one application, the resonator has been integrated with CMOS circuitry to form a micromechanical oscillator [11]. The resonator components are made entirely from the homogeneous, conducting,  $2\text{ }\mu\text{m}$ -thick polysilicon film. The spacer gap of  $2\text{ }\mu\text{m}$  above the substrate is set by the PSG thickness. The movable microstructure (in the center of the micrograph) is fixed to the substrate at only two points.

Simplified layout and schematic views of the device are shown in Fig. 3. The resonator is a

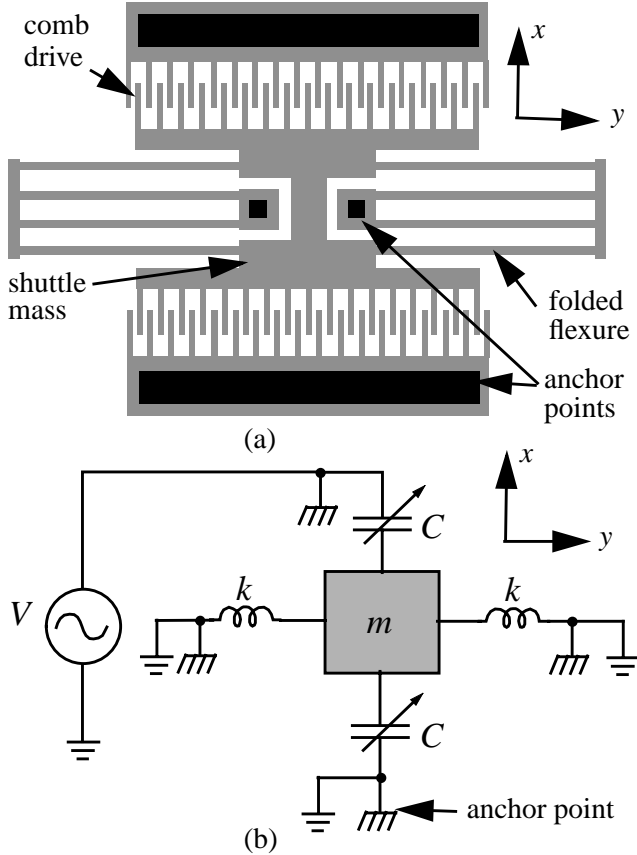


Fig. 3. Circuit-level views of the lateral folded-flexure comb-drive microresonator. (a) Physical view (layout). (b) Mixed-domain structural view (schematic), including a voltage source,  $V$ , for comb-

mechanical mass-spring-damper system consisting of a central shuttle mass that is suspended by two folded-beam flexures. The folded flexure is a popular design choice because it is insensitive to buckling arising from residual stress in the polysilicon film. Instead of buckling, the beams expand outward to relieve the stress in the film. The resonator is driven in the preferred ( $x$ ) direction by electrostatic actuators that are symmetrically placed on the sides of the shuttle. Each actuator, commonly called a ‘comb drive,’ are made from a set of interdigitated comb fingers. When a voltage is applied across the comb fingers, an electrostatic force is generated which, to first order, does not depend on  $x$ . The suspension is designed to be compliant in the  $x$  direction of motion and to be stiff in the orthogonal direction ( $y$ ) to keep the comb fingers aligned.

In the schematic view of Fig. 3.(b), the resonator is represented as an interconnected set of lumped-

parameter elements: the shuttle mass, two folded-flexure springs, and two comb-finger actuators which are displayed as time-varying capacitors. A voltage source that drives one actuator is included in the schematic.

Lateral translational modes of the mass-spring-damper system are modeled by second-order equations of motion:

$$F_{e,x} = m_x \ddot{x} + B_x \dot{x} + k_x x \quad (1)$$

$$F_{e,y} = m_y \ddot{y} + B_y \dot{y} + k_y y \quad (2)$$

where  $F_{e,x}$  and  $F_{e,y}$  are lateral components of the external electrostatic force generated by the comb drives. The effective masses ( $m_x$  and  $m_y$ ), damping coefficients ( $B_x$  and  $B_y$ ), and spring constants ( $k_x$  and  $k_y$ ) for these modes are calculated from the geometry and material parameters of the lumped elements. The vertical ( $z$ ) mode, rotational modes, and other higher order modes are left out of the present study because the equations unnecessarily complicate the analysis without providing for significantly greater insight into the design and synthesis issues.

### 2.3. Design Variables

All design variables of the microresonator are structural parameters of the folded flexure and comb drive elements, with the exception of the comb-drive voltage. The 14 variables used in the synthesis algorithm, along with upper and lower bounds, are listed in Table 1. Most of the layout parameters are detailed in Fig. 4. The choice of upper and lower bounds is discussed in the section on design constraints.

Several geometric variables, such as the width of the anchor supports,  $w_a$  and  $w_{as}$ , are not included in Table 1. These variables are necessary to completely define the layout, but do not affect the resonator behavior. We refer to these variables as ‘style’ parameters, because they primarily affect the stylistic look of the finished device.

Redundant state variables can be defined that depend on the design variables. For example, the shuttle axle length,  $L_{sa}$ , is a state variable which is dependent on the truss beam length and the gap between the beam anchor and the shuttle yoke. In our formulation of the problem, this gap is a style parameter.

Table 1. Design variables for the microresonator. Upper and lower bounds are in units of  $\mu\text{m}$  except  $N$  and  $V$ .

var.	description	min.	max.
$L_b$	length of flexure beam	2	400
$w_b$	width of flexure beam	2	200
$L_t$	length of truss beam	2	200
$w_t$	width of truss beam	4	400
$w_{sa}$	width of shuttle axle	11	400
$w_{sy}$	width of shuttle yoke	11	400
$L_{sy}$	length of shuttle yoke	84	400
$w_{cy}$	width of comb yoke	11	400
$L_c$	length of comb fingers	8	200
$w_c$	width of comb fingers	2	400
$g$	gap between comb fingers	2	100
$x_o$	comb finger overlap	4	100
$N$	number of comb fingers	15	100
$V$	voltage amplitude	5 V	50 V

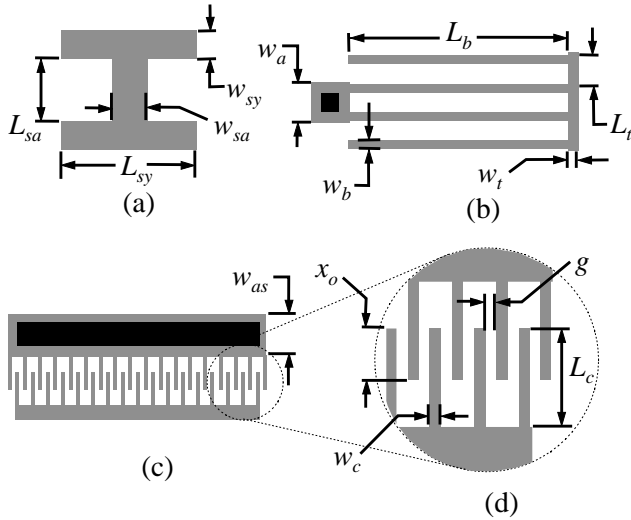


Fig. 4. Parameterized elements of the microresonator. (a) shuttle mass, (b) folded flexure, (c) comb drive with  $N$  movable 'rotor' fingers, (d) close-up view of comb fingers.

## 2.4. Lumped-Element Modeling

A very brief description of the models used in the synthesis algorithm are given in this section. The models for the spring constants, damping, and comb-drive force are derived in detail in the references listed with each equation.

The effect of spring mass on resonance is incorporated in an effective mass for the entire structure in each lateral direction.

$$m_x = m_s + \frac{1}{4}m_t + \frac{12}{35}m_b \quad (3)$$

$$m_y = m_s + \frac{8}{35}m_t + m_b \quad (4)$$

where  $m_s$  is the shuttle mass,  $m_t$  is the total mass of all truss sections, and  $m_b$  is the total mass of all long beams.

For operation at atmospheric pressure, damping is dominated by viscous air forces generated by the moving shuttle. Viscous air damping is proportional to velocity with a damping factor given by [12]

$$B_x = \mu \left[ (A_s + 0.5A_t + 0.5A_b) \left( \frac{1}{d} + \frac{1}{\delta} \right) + \frac{A_c}{g} \right] \quad (5)$$

where  $\mu$  is the viscosity of air,  $d$  is the spacer gap,  $\delta$  is the penetration depth of airflow above the structure,  $A_c$  is the gap between comb fingers, and  $A_s$ ,  $A_t$ ,  $A_b$ , and  $A_c$  are bloated layout areas for the shuttle, truss beams, flexure beams, and comb-finger sidewalls, respectively. Damping factors of the other lateral modes do not enter into the design constraints and are not calculated.

Linear equations for the folded-flexure spring constants in the lateral directions are [13]

$$k_x = \frac{2Et w_b^3}{L_b^3} \frac{L_t^2 + 14\alpha L_t L_b + 36\alpha^2 L_b^2}{4L_t^2 + 41\alpha L_t L_b + 36\alpha^2 L_b^2} \quad (6)$$

$$k_y = \frac{2Et w_t^3}{L_t^3} \frac{8L_t^2 + 8\alpha L_t L_b + \alpha^2 L_b^2}{4L_t^2 + 10\alpha L_t L_b + 5\alpha^2 L_b^2} \quad (7)$$

where  $E$  is the Young's modulus of polysilicon,  $t$  is the polysilicon thickness and  $\alpha = (w_t/w_b)^3$ .

General analytic equations for the lateral comb-drive force,  $F_x$ , as a function of  $w_c$ ,  $g$ ,  $t$ , and  $d$  are derived in [14], but are too lengthy to repeat here. For the special case of equal comb-finger width, gap, thickness, and spacing above the substrate ( $w_c = g = t = d$ ), each comb drive generates a force that is proportional to the square of the voltage,  $V$ , applied across the comb fingers.

$$F_{e,x} \cong 1.12\epsilon_o N \frac{t}{g} V^2 \quad (8)$$

where  $\epsilon_o$  is the permittivity of air. If the comb fingers are not perfectly centered, a  $y$ -directed electrostatic force is also present. Assuming a small perturbation  $y$  and that only one comb actuator is activated, the destabilizing force is found to be

$$F_{e,y} \approx 1.12\epsilon_o NV^2(x_o + x)ty/g^3 \quad (9)$$

### 3. LAYOUT SYNTHESIS

#### 3.1. Design Constraints

Several design specifications must be defined to constrain the layout synthesis of the microresonator. An essential specification is resonant frequency of the lowest mode ( $x$ ), which is determined by the spring constant and effective mass of the resonator.

$$f_x = \frac{1}{2\pi} \sqrt{\frac{k_x}{m_x}} \quad (10)$$

A valid layout must have a resonant frequency within 10% of the desired value. Resonant frequency of the orthogonal mode,  $f_y$ , is set at least 10 times greater than  $f_x$  to decouple the modes.

Specifications for minimum displacement and maximum applied voltage act as additional constraints. The displacement amplitude at resonance is related to the spring constant, damping, and comb-drive force. Assuming the system is underdamped, the displacement amplitude is

$$x_{max} = QF_x/k_x \quad (11)$$

where  $Q = \sqrt{m_x k_x / B_x^2}$  is the quality factor. We have constrained  $2 \mu\text{m} \leq x_{max} \leq 5 \mu\text{m}$  at a drive voltage of  $V < 50 \text{ V}$  to enable easy visual confirmation of resonance, and  $Q \geq 5$  to ensure underdamped resonant operation.

For stability, the restoring force of the spring in the  $y$  direction must be greater than the destabilizing electrostatic force from the comb drive.

$$F_{e,y} < k_y y \quad (12)$$

The layout is constrained by the MUMPs design rules. Several design rules set minimum beam widths and minimum spaces between structures. Maximum structure size is limited by undesirable curling due to stress gradients in the structural film and by possible

sticking and breakage during the wet release etch. We have constrained beam lengths to less than  $400 \mu\text{m}$  to avoid these problems.

If all the above constraints are met, then a design with minimum area can be found which is considered optimal.

#### 3.2. Synthesis Algorithm

In our approach, the synthesis problem is mapped onto a constrained optimization formulation that is solved in an unconstrained fashion. As in [15], the circuit design problem is mapped to the non-linear constrained optimization problem (NLP):

$$\left. \begin{array}{l} \min_{\underline{u}} \quad z = \sum_{i=1}^k w_i \cdot f_i(\underline{u}, \underline{x}) \\ \text{s.t.} \quad \underline{h}(\underline{u}, \underline{x}) = 0 \\ \quad \quad \underline{g}(\underline{u}, \underline{x}) \leq 0 \\ \quad \quad \underline{u} \in U_P \end{array} \right\} \text{(NLP)} \quad (13)$$

where  $\underline{u}$  is the vector of independent variables, such as geometries of micromachined devices that we wish to change to determine the MEMS structure performance;  $\underline{x}$  is the vector of state variables;  $\underline{f}(\underline{u}, \underline{x})$  is a set of objective functions that codify performance specifications the designer wishes to optimize, *e.g.*, area; and  $\underline{h}(\underline{u}, \underline{x}) = 0$  and  $\underline{g}(\underline{u}, \underline{x}) \leq 0$  are each a set of constraint functions that codify specifications that must satisfy a specific goal. For example, resonant frequency is constrained to greater than 20 kHz by the function  $20000 - f_x(\underline{u}, \underline{x}) \leq 0$ . Scalar weights,  $w_i$ , balance competing objectives. The decision variables can be described as a set  $\underline{u} \in U_P$ , where  $U_P$  is the set of allowable values for  $\underline{u}$  (described by the bounds in Table 1).

To allow the use of simulated annealing, we convert this constrained optimization problem to an unconstrained optimization problem with the use of additional scalar weights. As a result, the goal becomes minimization of a scalar cost function,  $C(\underline{u})$ , defined by

$$C(\underline{u}) = \sum_{i=1}^k w_i f_i(\underline{u}, \underline{x}) + \sum_{i=1}^l w_i' g_i(\underline{u}, \underline{x}) + \sum_{i=1}^m w_i'' h(\underline{u}, \underline{x}) \quad (14)$$

The key to this formulation is that the minimum of  $C(\underline{u})$  corresponds to the circuit design that best matches the given specifications. Thus, the synthesis task is divided into two sub-tasks: evaluating  $C(\underline{u})$  and searching for its minimum.

Evaluating the cost function involves firing the lumped-element macro-models to determine the extent to which the design constraints are met, for the current values of the design variables,  $\underline{u}$ . This cost function has multiple minima due to the complex non-linear characteristics of the individual equations in the lumped-element macro-model.

We use *simulated annealing* [16] as the optimization engine to drive the search for the minimum; it provides robustness and the potential for global optimization in the face of many local minima. Because annealing incorporates controlled *hill-climbing* it can escape local minima and is essentially starting-point independent.

#### 4. RESULTS AND DISCUSSION

Five lateral comb-drive resonator structures synthesized from specifications are shown in Fig. 1. For visualization of the synthesis results, we used the Consolidated Micromechanical Element Library (CaMEL) parameterized module generation software [17] from MCNC which provides CIF output when given resonator layout parameters. The CaMEL generators automatically place holes in the large plates that are over 30  $\mu\text{m}$  in size.

Several iterations of the design variables and constraints were necessary to produce synthesized designs that followed manual design convention and common sense. The layout visualization was instrumental in debugging the equations. Feedback from the synthesis iterations directed our efforts to codify the design variables and constraints. In many cases, a quick inspection of a synthesized layout is all that was need to determine errant or missing equations.

As expected, the devices shown in Fig. 1 become smaller with increasing values of resonant frequency.

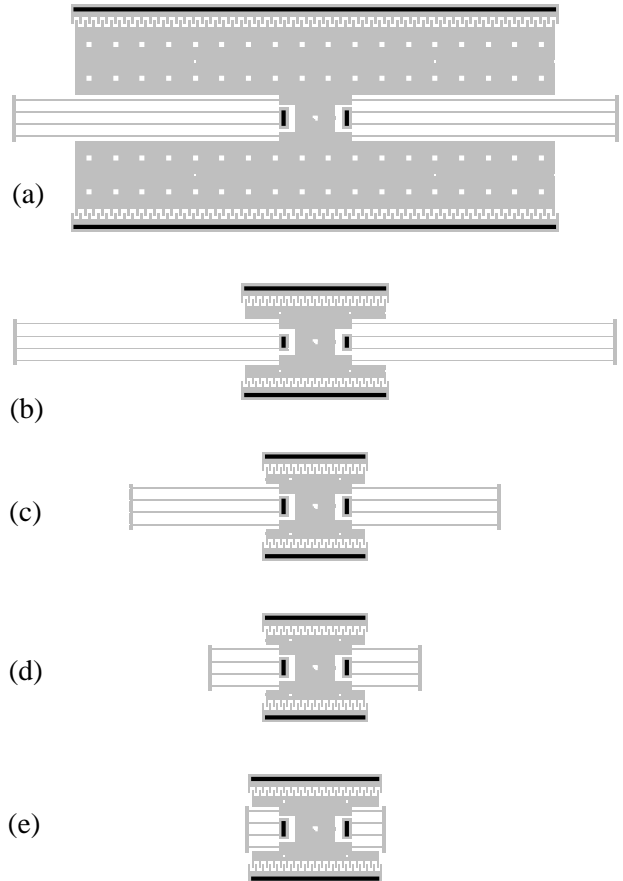


Fig. 1. Layout of five resonators synthesized from specifications. (a)  $f_r = 3$  kHz, (b) 10 kHz, (c) 30 kHz, (d) 100 kHz, (e) 300 kHz.

Smaller devices have less mass, and smaller flexures are stiffer. Both effects increase the resonant frequency. Values of selected design variables and behavioral parameters for the five resonator examples are given in Table 2.

For high frequency resonators, the mass becomes limited by the lower bounds on the shuttle mass and comb drive dimensions. The algorithm always chooses a device at the high end of the frequency specification, since that will yield a minimum size device. Quality factor is smaller for the larger resonators which have more air drag.

The maximum beam length is 400  $\mu\text{m}$ , however the 3kHz design is not able to take advantage of that due to the stylistic design constraint that the structure should be less than 700  $\mu\text{m}$  in the y-direction. In our formulation, the number of comb fingers,  $N$ , is tied directly to the shuttle size. Therefore,  $N$  is large for

Table 2. Selected behavioral and physical parameters for the five synthesized resonators.

Spec. [kHz]	3±0.3	10±1	30±3	100±10	300±30
$m_x$ [ng]	435.	39.9	25.7	23.4	26.7
$L_b$ [μm]	304	302	168	77	36
$k_x$ [N/m]	0.187	0.191	1.10	11.2	122.
$f_x$ [kHz]	3.30	11.0	33.0	110	340
$Q$	9.35	20.0	56.2	181	503
$N$	50	21	15	15	19
$V$ [V]	14.0	15.0	25.5	45.1	50.0
$x_{max}$ [μm]	4.97	5.00	5.00	4.99	1.93
$V_{crit}$ [V]	9190	14200	16700	16500	15300

the low-frequency (large mass) resonators. Very low frequency resonators are limited by the upper bounds imposed on geometry. The upper bound on displacement amplitude of 5 μm is achieved for all of the devices in Fig. 1 except the 300 kHz resonator. The optimization does not directly evaluate all the equations in each iteration. Instead it builds a local low-order macro-model of the equations which is regularly updated. This can sometimes lead to the optimizer believing it has met a constraint when post-synthesis simulation (used to generate the performance numbers in Table 2) indicates that the optimizer actually overshot the constraint. This occurred in the resonant frequency and maximum displacement specifications of the 300 kHz design.

Note that although  $N$  is more than doubled from the 10 kHz to 3 kHz device, the  $Q$  is reduced by about 1/2. Therefore, the applied voltage stays nearly constant for these devices. The lower limit for  $N$  (=15) is reached for intermediate frequency resonators. For high-frequency resonators, the voltage limit is reached and  $N$  must be increased to provide adequate electrostatic force to achieve the 2 μm minimum displacement. Very high frequency resonators cannot be synthesized because the necessary increase in comb fingers generates a more massive device, which drives the resonant frequency down.

A critical voltage,  $V_{crit}$ , is defined as the applied voltage necessary to crash the movable comb fingers into the stator comb fingers. The values for  $V_{crit}$  in Table 2 are much larger than any voltages experienced

by the resonators. However, the first-order spring model in our analysis does not account for spring softening for non-zero values of  $x$  deflection. More realistic models may raise the significance of this 2D constraint.

## 5. CONCLUSIONS

Synthesis algorithms have been successfully applied to automatic layout of surface-micromachined resonators. A prerequisite for synthesis is a set of lumped-parameter models that adequately link device behavior with physical design variables. One great benefit of creating synthesis tools is that it forces the CAD developer to codify every design variable and design constraint.

Once a structured design methodology is established for surface-micromachined MEMS, the synthesis techniques may be extended to general parameterized designs. Then we can integrate structural synthesis with electronic design using the similar formulation for circuits in [4]. Our long-term goal is to enable rapid, intuitive exploration and analysis of the design space for MEMS.

## ACKNOWLEDGEMENT

The authors thank Karen Markus and Ramaswamy Mahadevan of MCNC for use of the CaMEL tool.

## REFERENCES

- [1] S. D. Senturia, R. Harris, B. Johnson, S. Kim, K. Nabors, M. Shulman, and J. White, "A Computer-Aided Design System for Microelectromechanical Systems," *J. of Microelectromechanical Systems*, v.1, no.1, pp. 3-13, Mar. 1992.
- [2] IntelliCAD, IntelliSense Corporation, 16 Upton Dr., Wilmington, MA 01887.
- [3] S. B. Crary, O. Juma, and Y. Zhang, "Software Tools for Designers of Sensor and Actuator CAE Systems," *Technical Digest of the IEEE Int. Conference on Solid-State Sensors and Actuators (Transducers '91)*, San Francisco, CA, pp. 498-501, June 1991.
- [4] T. Mukherjee, L.R. Carley, and R.A. Rutenbar, "Synthesis of Manufacturable Analog Circuits," *Proceedings of ACM/IEEE ICCAD*, pp. 586-593, Nov '94.

- [5] I. E. Grossmann and D. A. Straub, "Recent Developments in the Evaluation and Optimization of Flexible Chemical Processes," *Proceedings of COPE-91*, pp 49-59, 1991.
- [6] D. A. Koester, R. Mahadevan, K. W. Markus, *Multi-User MEMS Processes (MUMPs) Introduction and Design Rules*, available from MCNC MEMS Technology Applications Center, 3021 Cornwallis Road, Research Triangle Park, NC 27709, rev. 3, Oct. 1994, 39 pages.
- [7] J. T. Kung and S. Lewis, *BiMOS Technology Stage One Design Rules*, Analog Devices, 831 Woburn St., Wilmington, MA 01887, 14 pages (available from <http://www-mtl.mit.edu:8001/htdocs/starting.html>).
- [8] *Micromachines Program*, available from Multi-Project Circuits (CMP) Service, 46, avenue Felix Viallet, 38031 Grenoble Cedex, Oct. 1994, 29 pages.
- [9] G. K. Fedder, S. Santhanam, M. L. Reed, S. Eagle, D. Guillou, M. S.-C. Lu, and L. R. Carley, "Laminated High-Aspect-Ratio Microstructures in a Conventional CMOS Process," *Proceedings of the IEEE Micro Electro Mechanical Systems Workshop*, San Diego, CA, pp. 13-18, Feb. 1996.
- [10] W. C. Tang, T.-C. H. Nguyen, M. W. Judy, and R. T. Howe, "Electrostatic Comb Drive of Lateral Polysilicon Resonators," *Sensors and Actuators A*, vol.21, no.1-3, pp. 328-31, Feb. 1990.
- [11] C. T.-C. Nguyen and R. T. Howe, "CMOS Micromechanical Resonator Oscillator," *Technical Digest of the IEEE Int. Electron Devices Meeting*, Washington, D.C., pp. 199-202, 1993.
- [12] X. Zhang and W. C. Tang, "Viscous Air Damping in Laterally Driven Microresonators," *Proceedings of the IEEE Micro Electro Mechanical Systems Workshop*, Oiso, Japan, pp.199-204, Jan. 1994.
- [13] G. K. Fedder, *Simulation of Microelectromechanical Systems*, Ph.D. Thesis, Dept. of Electrical Engineering and Computer Science, University of California at Berkeley, Sept. 1994.
- [14] W. A. Johnson and L. K. Warne, "Electrophysics of Micromechanical Comb Actuators," *J. of Microelectromechanical Systems*, v.4, no.1, pp.49-59, Mar. 1995.
- [15] E. S. Ochotta, R. A. Rutenbar, and L. R. Carley, "ASTRX/OBLX: Tools for Rapid Synthesis of High Performance Analog Circuits," *Proc. 31st ACM/IEEE DAC*, pp. 24-30, June 1994.
- [16] S. Kirkpatrick, C. D. Gelatt, and M. P. Vecchi, "Optimization by Simulated Annealing," *Science*, vol. 220, no. 4598, May 1983.
- [17] *CaMEL Web Page*, <http://www.mcnc.org/camel.org>, MCNC MEMS Technology Applications Center, 3021 Cornwallis Road, Research Triangle Park, NC 27709.